

# SPACE-CHARGE AND OTHER EFFECTS IN FERMILAB BOOSTER AND IOTA RINGS' IONIZATION PROFILE MONITORS \*

V. Shiltsev<sup>†</sup>, Fermi Accelerator Laboratory, Batavia, IL, USA

## Abstract

Ionization profile monitors (IPMs) are widely used in accelerators for non-destructive and fast diagnostics of high energy particle beams. At low beam intensities, initial velocities of the secondaries to collect (ions or electrons) result in the IPM profile smearing. At high beam intensities, the space-charge forces make the measured IPM profiles significantly different from those of the beams. We analyze dynamics of the secondaries in IPMs, describe an effective algorithm to reconstruct the beam sizes from the measured IPM profiles and apply it to the Fermilab 8 GeV proton Booster and 70 MeV/c IOTA ring IPMs.

## INTRODUCTION

Particle accelerators heavily rely on precise diagnostics and control of critical beam parameters such as intensity, pulse structure, position, transverse and longitudinal beam sizes, halo, etc [1]. Ionization profile monitors (IPMs) [2–7] are fast and non-destructive diagnostic tools used in proton and ion linacs, colliders, and rapid cycling synchrotrons (RCS) [8–10]. They operate by collecting ions or electrons created after the ionization of residual vacuum molecules by high energy charged particle beams [1, 11], which are then guided to a detector by a uniform external electric field  $E_{\text{ext}}$ . The detector is usually made of many thin parallel strips, whose individual signals are registered to make the beam profile signal ready for processing – see Fig.1.

Space-charge forces of the primary beams make the measured IPM profiles different from those of the beams and must be correctly accounted for. Brute force numerical modeling [12, 13] can successfully reproduce experimentally measured IPM profiles but offer limited predictive physics insights. Several phenomenological fits were proposed to relate the measured beam size  $\sigma_m$  and the initial beam size  $\sigma_0$  - see, e.g., [3, 12, 14, 15] - but despite acceptable data approximation, they are not based on clear physical reasons for as many four free parameters and exponents. Below we briefly describe an effective algorithm developed in [16] to reconstruct the beam sizes from measured IPM profiles and known key parameters, such as high-energy beam intensity  $N$  and IPM extracting field  $E_{\text{ext}}$  is the guiding electric field. Based on that theory, we discuss the Booster IPMs measurements and possible upgrades, as well as specifications for the IOTA ring IPMs.

\* This manuscript has been authored by Fermi Research Alliance, LLC under Contract No. DE-AC02-07CH11359 with the U.S. Department of Energy, Office of Science, Office of High Energy Physics.

<sup>†</sup> shiltsev@fnal.gov

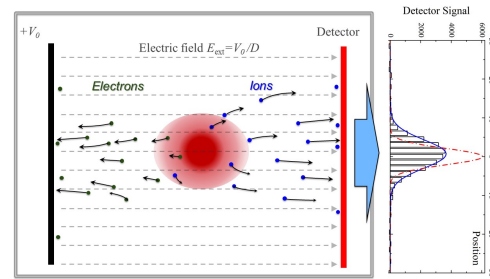


Figure 1: Transverse cross-section of a high energy beam (red) in vertical IPM and schematically shown motion of secondary ions (blue dots) and electrons (green dots) under the impact of horizontal extracting electric field  $E_{\text{ext}}$  and space-charge field of the primary beam. The diagram on the right shows the IPM detector signals at right before extraction of an intense beam of  $N = 4.6 \cdot 10^{12}$  protons from the Fermilab Booster synchrotron. The actual rms proton vertical size of the proton beam is  $\sigma_0 = 2.1$  mm - see dashed red curve, while the rms width of the IPM signal is  $\sigma_m = 3.6$  mm, see blue line for the Gaussian fit.

## SPACE-CHARGE DRIVEN IPM PROFILE EXPANSION

Ref. [16] presents a final-form solution of the general equations of transverse motion of non-relativistic ions with charge  $Ze$  and mass  $M$  born in the acts of ionization of the residual gas molecules by a high energy proton beam passing through IPM with extracting external electric field  $E_{\text{ext}} = V_0/D$  due to the voltage gradient  $V_0$  across the IPM gap  $D$ . No guiding external magnetic field is assumed. IPMs usually operate with electric fields  $E_{\text{ext}} \sim O(100-1000 \text{ V/mm})$  which significantly exceed the space-charge field  $E^{\text{SC}} \sim O(1-10 \text{ V/mm})$  and that assumption helps to solve the equations of motion.

Important beam parameters of the high energy beam are its current  $J(t)$ , velocity  $v_p$  and rms transverse size  $\sigma_0$ . The space-charge potential of such beam is  $U_{\text{SC}} = J/(4\pi\epsilon_0 v_p) \approx 30[\text{V/A}]J/\beta_p$ ,  $\beta_p = v_p/c$ ,  $c$  is the speed of light, and  $\epsilon_0$  is the permittivity of vacuum [17]. Three characteristic times are of importance for the analysis: i) a characteristic time for the secondaries to get extracted out of the beam by the external electric field  $\tau_0 = \sqrt{\frac{2M\sigma_0}{ZeE_{\text{ext}}}} = \tau_2 \sqrt{\frac{\sigma_0}{d}}$ ; ii) time for secondary particle to reaches the IPM detector plane  $\tau_2 = \sqrt{\frac{2Md}{ZeE_{\text{ext}}}}$ , where  $d$  is the average distance from the beam center to the detector; and iii) a characteristic expansion time due to the space-charge  $\tau_1 = \left(\frac{eZU_{\text{SC}}}{M\sigma_0^2}\right)^{-1/2}$ .

Proton beam space-charge fields result in *proportional magnification of the IPM profile* of the distribution of the secondary particles, i.e.,  $\sigma_m = \sigma_0 \cdot h$ . Under a reasonable

assumption of DC or slow varying proton current  $J(t) = J$ , the rms transverse size of the IPM profile at the time when the secondary particle reaches the IPM detector  $t = \tau_2 \gg \tau_0$  is found as:

$$\sigma_m = \sigma_0 \cdot h \approx \sigma_0 \cdot \left[ 1 + \frac{2U_{SC}}{E_{ext}\sigma_0} \left( \frac{\Gamma(\frac{1}{4})}{3} \sqrt{\frac{d}{\sigma_0}} - \frac{\sqrt{\pi}}{2} \right) \right]. \quad (1)$$

The gamma-function  $\Gamma(\frac{1}{4}) \approx 3.625$ . The space-charge magnification factor  $h$  is determined only by the space-charge potential  $U_{SC}$ , the primary beam size  $\sigma_0$ , the IPM extracting field  $E_{ext}$ , and the beam-to-MCP distance  $d$  but *it does not depend on the type of secondary species* (their mass and charge, etc). Equation (1) can be easily solved, and the original  $\sigma_0$  can be found from  $\sigma_m$  with other IPM and beam parameters known.

A similar analysis for uniform, rather than Gaussian, primary proton beam current density distribution with radius  $a$  results in an exact solution in elementary functions that is very close to Eq. (1), with the numerical factor  $2\Gamma(1/4)/3 \approx 2.42$  replaced by  $(4\sqrt{2}/3) \approx 1.88$ , and substitution of equivalent  $\sigma_0 = a/2$ .

The effect of the high-energy beam current  $J(t)$  time structure, such as in bunched beams, depends on the rms bunch length  $\tau_b$  and time between bunches  $t_b$  and can be approximated by substitution  $U_{SC} \rightarrow U_{SC}(1 + t_b/\tau_0)$ . See [16] for details as well analysis of the extreme case of short and rare bunches  $\tau_b \ll (\tau_0, \tau_1, \tau_2) \ll t_b$ .

The effect of the high energy beam size aspect ratio  $R = \sigma_x/\sigma_y$  is relatively weak, too. Indeed, the space-charge factor  $1/\tau_1^2$  scales as  $2/(1+R)$  while the characteristic time  $\tau_0 \propto \sqrt{R}$ . Therefore, the magnification factor  $H$  – which is proportional to the product  $\tau_0/\tau_1^2$  – scales as  $2\sqrt{R}/(1+R)$ . The latter is relatively small, i.e. 0.94 for  $R = 0.5$ , and can be safely neglected for most common cases of  $h \leq 2$ .

To account for initial velocities of the secondaries  $v_{0,y}$ , one can assume them to be random with the rms value of  $\sqrt{2\mathcal{E}_i/M}$  and get in quadrature addition to Eq. (1):

$$\sigma_m^2 = \sigma_0^2 h^2 (U_{SC}, \sigma_0, E_{ext}, d) + \left( \frac{4\mathcal{E}_i d}{ZeE_{ext}} \right). \quad (2)$$

The types of IPMs are distinguished by the species they collect - electrons or ions. The initial kinetic energy  $\mathcal{E}_i$  for ionization electrons is about 35 eV needed on average for ion-electron pair production by protons in hydrogen [18]. Corresponding smearing Eq. (2) of the particle position measured by the IPM is about  $\sigma_T = D\sqrt{2\mathcal{E}_i/ZeV_0}$ , that is some 6 mm for a typical gap  $D = 100$  mm and voltages as high as  $V_0 = 20$  kV. That is absolutely unacceptable for millimeter-scale or smaller primary beam sizes and the electron-collecting IPMs usually have to use a focusing external magnetic field  $B_x$ , parallel to the extracting electric field, to suppress the smearing. Physics principles, advantage, and disadvantages of the IPMs with a magnetic field are discussed in [19].

As for ions, their initial kinetic energy is smaller and depends on their kind and the type of reaction. For diatomic gases, the most relevant process is dissociative ionization by the primary fast protons, i.e.,  $p + H_2 \rightarrow p + H + H^+$  with typical kinetic energy of the  $H^+$  of the order of a few eV [20]. Corresponding smearing of the profile  $\sigma_T$  in the ion-collecting IPMs is  $O(1 \text{ mm})$  [21]. These IPMs do not require an external magnetic field and, therefore, are usually of smaller size, simpler design, and lower cost. Two such monitors – vertical and horizontal – are installed in the Fermilab Booster rapid cycling synchrotron (RCS) and we apply our analysis to their experimentally measured profiles [22, 23].

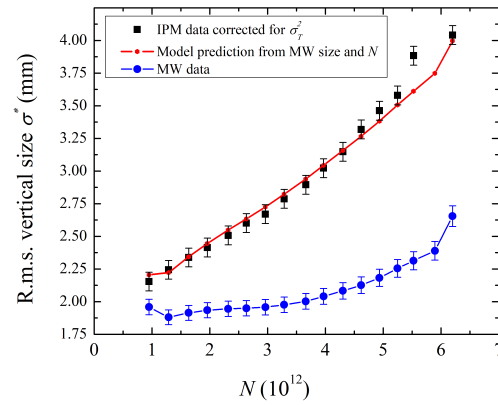


Figure 2: The Fermilab Booster IPM vertical rms beam size  $\sigma^*$  right before beam extraction ( $V_0 = 24$  kV,  $D = 103$  mm, black squares) [16, 22] vs the total proton beam intensity  $N$ . The theoretical prediction of this paper's Eq. (1) (red line) is calculated using the initial beam sizes  $\sigma_0$  as measured by the Multi-Wires emittance monitor (blue line). The measured IPM rms sizes  $\sigma_m$  are corrected for the intensity independent smearing  $\sigma^* = \sqrt{\sigma_m^2(N) - \sigma_T^2}$ , with  $\sigma_T^2 = 2.7 \text{ mm}^2$ .

## APPLICATION FOR FERMILAB BOOSTER IPM

The Fermilab Booster [24] is a 474 m circumference, alternating-gradient 15 Hz RCS accelerating protons from 0.4 GeV at injection to 8.0 GeV at extraction in 33.3 ms, or about 20,000 turns – half of the magnet cycle period. Correspondingly, all proton beam parameters (intensity, positions, bunch length, emittances) as well as accelerating RF frequencies and voltage significantly vary in the cycle. The typical total intensity of 84 circulating proton bunches is about  $N = 4.6 \cdot 10^{12}$ . The Booster proton beam dynamics is quite complex leading to the beam emittance growth and particle losses during the acceleration [22] which set limits on the high power operation of the entire Fermilab complex of accelerators for high energy neutrino physics [25, 26]. Fast diagnostics of the proton beam size is, therefore, of critical importance for the Booster operations and upgrades.

There are two types of instruments to measure beam sizes in the Booster – the Multi-Wires and IPMs. The Multi-Wires are intercepting devices installed in the Booster extraction beamline. The Multi-Wires (harps of 48 wires spaced by 1 mm) beam size measurements data are presumed to be intensity independent and accurate to some 2-3%. The IPMs operate in the ion collection mode and report the average rms beam sizes (determined by the Gaussian fits of the profiles) every turn (about 2  $\mu$ s).

Besides the space-charge expansion and the effect of the initial ion velocities Eq. (2), the IPM intensity independent profile smearing can be caused by a finite separation between the individual IPM charge collection strips (total of 40,  $\Delta = 1.5$  mm apart), angular misalignment of the long and narrow strips with respect to the high energy beam trajectory, and by non-uniformity of the extraction electric field in the operational IPM aperture and these effects can be taken into account by cross-calibration of low-intensity beam sizes measured by the IPM  $\sigma_m$  and by the Multi-Wires  $\sigma_{MW}$ , or by other appropriate beam size monitors [1, 9, 22, 27–30]. Comparison of the Booster IPM and Multi-Wires data at various beam intensities yields  $\sigma_T^2 = \lim_{N \rightarrow 0} (\sigma_m^2(N) - \sigma_{MW}^2(N)) = 2.8 \pm 0.1 \text{ mm}^2$  [22].

At high intensity, the average space-charge potential of the Booster proton beam is  $U_{SC} \approx 14[\text{V}] \cdot N / (4.6 \cdot 10^{12})$ . Typical rms proton bunch length and bunch-to-bunch spacing are  $\tau_b \approx 2 - 3$  ns,  $t_b \approx 19$  ns. Characteristic times for the IPM with  $D = 103$  mm and  $V_0 = 24$  kV are  $\tau_b \approx 2 - 3$  ns,  $t_b \approx 19$  ns,  $\tau_0 \approx 22$  ns,  $\tau_1 \approx 67$  ns (for  $N = 6 \cdot 10^{12}$ ) and  $\tau_2 \approx 110$  ns. Therefore, the beam profile expansion factor  $h$  can be calculated by using Eq. (1) in which the original  $\sigma_0$  is taken from the Multi-Wires data and with the beam-to-MCP distance  $d \approx D/2 = 52$  mm. To take into account the time structure of the Booster bunched beam, the rms profile expansion coefficient  $h$  Eq. (1) needs to be augmented by a numerical factor  $[1 + t_b/\tau_0]$ . The resulting rms vertical IPM beam size estimates  $h\sigma_0$  are found to be in excellent agreement with the measured IPM rms sizes  $\sigma^* = \sqrt{\sigma_m^2(N) - \sigma_T^2}$  measured over a broad range of beam intensities as illustrated in Fig. 2. One can see that the space-charge induced IPM profile expansion of the extracted beam (8 GeV proton kinetic energy) grows with the beam intensity and become quite large,  $h - 1 \approx 0.7$ , at the nominal  $N$ . The instrumental smearing  $\sigma_T$  adds another  $\sim(10-15)\%$ . For operational monitoring of the emittance evolution over the 33 ms acceleration ramp, it is important to account for : a) the beam orbit motion as the space-charge expansion depends on the distance  $d$  from the beam orbit to the IPM collection plate; b)  $O(10\%)$  variations of the beta-functions at the IPM locations during the ramp; c) significant changes in the beam bunching factor.

Knowing  $\sigma_T, N$  and the IPM extracting field  $V_0/D$  one can easily reverse Eq. (1) and find the original proton beam  $\sigma_0$  from the measured and corrected  $\sigma^*$ , see, e.g., [22]. Figure 3 illustrates the result of such analysis for the measured profiles of the Booster beam with  $N = 4.62 \cdot 10^{12}$ . There,

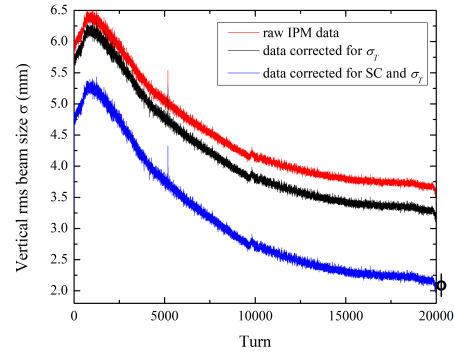


Figure 3: An example of reconstruction of vertical rms proton beam size in 33 ms (20000 turns) acceleration cycle of the Fermilab 8 GeV Booster synchrotron with the total beam intensity of  $N = 4.6 \cdot 10^{12}$ : time dependence of the original IPM data (red), the data corrected for smearing effects due to  $\sigma_T$  (black) and the same data after additional correction for the space-charge expansion (blue). The open black circle with error bars at the left represents the measured Multi-Wires beam size of the extracted beam.

the red curve is for the rms vertical beam size  $\sigma_m(t)$  as measured by the IPM at each of 20 thousand turns of the Booster acceleration cycle; the black line represents the beam size after correction for the intensity independent smearing  $\sigma^*$ ; and, finally, the true proton rms beam size  $\sigma_0$  was reconstructed following the algorithm of Eqs. (1) and (2) and is represented by the blue line. One can see that the overall beam size correction is about 20% early in the Booster acceleration cycle when the true rms beam size  $\sigma_0$  is about 5.3 mm. At the end of the acceleration cycle from 400 MeV to 8 GeV, accounting for the space-charge effect results in a very large correction from 3.7 mm to 2.2 mm rms. Also, one can see that the reconstructed IPM size at the end of the acceleration cycle matches well the extracted beam size measured by the Multi-Wires, as indicated by a black open circle with error bars at the right of Fig. 3.

## IPMS FOR BOOSTER UPGRADE AND IOTA

There are plans to further upgrade the Fermilab proton complex from the current world-leading level of  $\sim 840$  kW of average 120 GeV proton beam power on the neutrino target to over 1.2 MW at the start of the LBNF/DUNE experiment in the second half of the 2020s via replacement of the existing 40 years old 400 MeV normal-conducting Linac with a modern CW-capable 800 MeV superconducting RF linear accelerator (PIP-II, see [31]). The corresponding upgrade of the Booster IPMs will be needed, too, for two reasons. First of all, the PIP-II linac will provide about 50% increase in the Booster beam intensity to some  $N = 6.5 \cdot 10^{12}$  and, consequently, the IPM space-charge expansion factor will grow to  $h \approx 2.0$  making it very hard to account for it and correct. Secondly, recent experimental studies of the Booster

losses and emittance evolution [22, 23, 32] indicate a very complicated dynamics of the proton beam that includes a complex interplay of impedance, instabilities, space-charge effect, and electron cloud effects, many of which are manifested in significant differences in the behavior of individual bunches. The existing Booster IPMs have limited frequency bandwidth and are capable of reporting only one-turn average beam profiles, i.e., they can not measure profiles of individual bunches or groups of 6-10 bunches (out of 81-84 total).

Table 1: Parameters of Fermilab IPMs

	Tevatron*	Booster	IOTA
Proton $p_c$ , GeV	980	0.95-8.9	0.07
$N_p$ /bunch, $10^{10}$	25	5.5	9
$N_b$	36	84	1 or 4
$f_{rev}$ , $\mu$ s	21	2.22	1.83
$\beta_p$	1	0.7-1	0.07
$J_{avg}$ , mA	80	330	2-8
$U_{SC}$ , V	2.4	14	2.5
$t_b$ , ns	396	25-20	460-1800
$\sigma_p$ at IPM, mm	1-0.3	5-2	1-4
IPM $B$ , T	0.2	0	0
IPM $V_0$ , kV	10	24	24
IPM $D$ , mm	87	103	103
IPM pitch $\Delta$ , mm	0.25	1.5	0.5
IPM $h - 1$ , max.	$\sim 0.02$	$\sim 0.7$	$\sim 0.16$

A possible way to address the above needs might be the employment of the Tevatron-style IPMs [7, 9, 33–35] - see Table 1. Two of those (vertical and horizontal) were used in 2006-2011 (now in storage), operated in the electron collection mode with external guiding magnetic field  $B = 0.1 - 0.2$ T, had fast electronics and were able to report profiles of individual proton and antiproton bunches separated by some 200 ns. The guiding magnetic field effectively suppresses the space charge IPM profile expansion which otherwise would be as high as  $h \approx 1.6$ . The Larmor motion of electrons adds very little to the measured beam profile smearing, and the measured IMP beam profile was found to be very close, withing few %, to the real one with approximate relation  $\sigma_m = \sqrt{\sigma_0^2 + \delta_L^2/B^2}$ , where  $\delta_L \approx 26 \mu\text{m}$  at  $B = 1$  T [33]. For the such IPMs in the Booster, the field as low as  $B = 0.02$  T will suffice to keep the IPM smearing under  $\sim 10\%$ . To avoid beam orbit distortion due the IPMs, its integrated magnetic field  $\int B dl \approx 4 \cdot 10^{-3}$  Tm can be easily compensated or corrected.

No magnetic field, Booster-type IPMs can be employed for proton beam diagnostics in the IOTA ring [36]. Major parameters of that facility for accelerator research are listed in Table 1. One can see that even for the highest proton beam current and the smallest beam size - parameters which usually anti-correlate - the space-charge IPM expansion parameter is at about 16% that leaves enough room for reasonably precise correction following recipes of Eq.(1) and the above analysis. The revolution frequency of IOTA is

close to that of the Booster and the bandwidth of the existing Booster IPM electronics should be sufficient for turn-by-turn profile measurements in IOTA. Of course, for the rms beam size of about  $\sigma_0 \approx 1$  mm it would be very necessary to have a smaller pitch  $\Delta$  (distance between stripes), preferably 1 to 0.5 mm or less as it adds to the measured size in quadrature approximately as  $\sigma_m = \sqrt{\sigma_0^2 + \Delta^2}/12$ . Another attractive opportunity for improvement can be a controlled leak of Xe or Kr - see Fig.4 - as IPM operation with such gases results in a smaller profile smearing [21, 37].

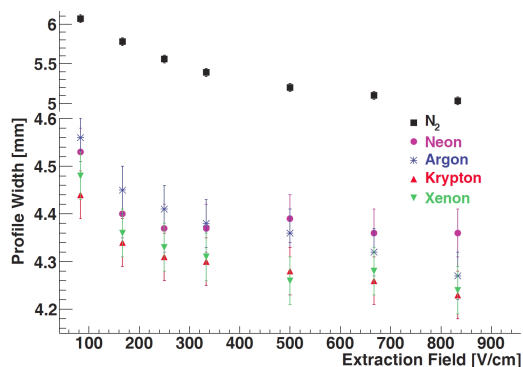


Figure 4: Measured GSI IPM profile width versus extraction field for different residual gases (from Ref. [37]).

## SUMMARY

Theory and analysis of space-charge effects and intensity independent instrumental errors  $\sigma_T$  in the operation of ionization profile monitors for measurements of high-intensity beams [16] offer practical correction algorithms to reconstruct the original beam sizes. Being applied to the 8 GeV Fermilab Booster proton synchrotron, that allows some 10% accuracy in the determination of  $\sigma_0$  from the rms sizes measured in the IPMs  $\sigma_m$ . Upcoming Booster beam intensity upgrade, besides expected increase in the IPM space-charge expansion factor up to  $\sim 2$ , rises concerns over multi-bunch proton dynamics effects - all that calls for the installation of faster IPMs which also employ some 0.02T guiding external magnetic field for electron collection. The Booster type (ion collecting) IPMs can be employed in the 70 MeV/c IOTA proton ring, especially if the pitch of the stripes can be reduced to 1 mm or less and the residual gas to ionize is set by calibrated Xe or Kr leaks.

The author would like to thank J. Eldred, V. Kapin, V. Lebedev, K. Seiya, and R. Thurman-Keup for useful discussions on various aspects of the Fermilab Booster IPM operation, fruitful cooperation, and valuable input.

## REFERENCES

- [1] P. Strehl, *Beam Instrumentation and Diagnostics*, vol. 120, Berlin, Germany: Springer, 2006.
- [2] F. Hornstra, W. H. DeLuca, "Nondestructive beam profile detection systems for the Zero Gradient Synchrotron", in *Proc. VI Conference on High Energy Acceleration*, Cambridge, MA, 1967, pp. 374–377.

- [3] H. Weisberg *et al.*, “An ionization profile monitor for the Brookhaven AGS”, *IEEE Trans. Nucl. Sci.*, vol. 30, p. 2179, 1983. doi:10.1109/TNS.1983.4332753
- [4] B. Hochadel *et al.*, “A residual-gas ionization beam profile monitor for the Heidelberg Test Storage Ring TSR”, *Nucl. Instr. Meth. A*, vol. 343, p. 401, 1994. doi:10.1016/0168-9002(94)90217-8
- [5] R. Anne *et al.*, “A noninterceptive heavy ion beam profile monitor based on residual gas ionization”, *Nucl. Instr. Meth. A*, vol. 329, p. 21, 1993. doi:10.1016/0168-9002(93)90918-8
- [6] R. Connolly *et al.*, “Beam profile measurements and transverse phase-space reconstruction on the Relativistic Heavy-Ion Collider”, *Nucl. Instr. Meth. A*, vol. 443, p. 2015, 2000. doi:10.1016/S0168-9002(99)01162-6
- [7] A. Jansson *et al.*, “The Tevatron ionization profile monitors”, *AIP Conf. Proc.*, vol. 868, p. 159, 2006. doi:10.1063/1.2401401
- [8] F. Benedetti *et al.*, “Design and development of ionization profile monitor for the cryogenic sections of the ESS Linac”, *EPJ Web of Conf.*, vol. 225, p. 01009, 2020. doi:10.1051/epjconf/202022501009
- [9] R. S. Moore, A. Jansson, and V. Shiltsev, “Beam instrumentation for the Tevatron collider”, *J. Instrumentation*, vol. 4, no. 12, p. 12018, 2009. doi:10.1088/1748-0221/4/12/P12018
- [10] S. Lévassieur *et al.*, “Development of a rest gas ionisation profile monitor for the CERN Proton Synchrotron based on a Timepix3 pixel detector”, *J. Instrumentation*, vol. 12, no. 02, p. C02050, 2017. doi:10.1088/1748-0221/12/02/C02050
- [11] K. Wittenburg, “Specific instrumentation and diagnostics for high-intensity hadron beams”, in *CAS - CERN Accelerator School: High Power Hadron Machines*, Mar. 2013, pp. 251–308. doi:10.5170/CERN-2013-001.251
- [12] J. Amundson *et al.*, “Calibration of the FNAL Booster ionization profile monitor”, *Phys. Rev. ST Accel. Beams*, vol. 6, p. 102801, 2003. doi:10.1103/PhysRevSTAB.6.102801
- [13] Workshop in Simulations, Design and Operational Experience of Ionisation Profile Monitors. <https://indico.gsi.de/event/5366>
- [14] R. Thern, “Space charge distortion in the Brookhaven ionization profile monitor”, BNL, Upton, NY, USA, Rep. BNL-39487, Mar. 1987.
- [15] W.S. Graves *et al.*, “A nondestructive fast beam profile monitor”, *Nucl. Instr. Meth. A*, vol. 364, p. 364, 1995. doi:10.1016/0168-9002(95)00218-9
- [16] V. Shiltsev, “Space-charge effects in ionization beam profile monitors”, *Nucl. Instr. Meth. A*, vol. 986, p. 164744, 2021. doi:10.1016/j.nima.2020.164744
- [17] M. Reiser, *Theory and Design of Charged Particle Beams*, New York, USA: John Wiley and Sons, 2008.
- [18] C. Bakker and E. Segre, “Stopping power and energy loss for ion pair production for 340-Mev protons”, *Phys. Rev.*, vol. 81, p. 489, 1951. doi:10.1103/PhysRev.81.489
- [19] D. Vilsmeier, M. Sapinski, and R. Singh, “Space-charge distortion of transverse profiles measured by electron-based ionization profile monitors and correction methods”, *Phys. Rev. Accel. Beams*, vol. 22, p. 052801, 2019. doi:10.1103/PhysRevAccelBeams.22.052801
- [20] C. Dimopoulou *et al.*, “Dissociative ionization of H<sub>2</sub> by fast protons: three-body break-up and molecular-frame electron emission”, *J. Phys. B: At. Mol. Opt. Phys.*, vol. 38, p. 593, 2005. doi:10.1088/0953-4075/38/5/010
- [21] J. Egberts, “IFMIF-LIPAC beam diagnostics. Profiling and loss monitoring systems”, Ph.D. thesis, Université Paris Sud, Orsay, France, 2012.
- [22] J. Eldred *et al.*, “Beam intensity effects in Fermilab Booster synchrotron”, *Phys. Rev. Accel. Beams*, vol. 24, p. 044001, 2021. doi:10.1103/PhysRevAccelBeams.24.044001
- [23] V. D. Shiltsev, J. S. Eldred, V. A. Lebedev, and K. Seiya, “Beam Losses and emittance growth studies at the Record high space-charge dQ\_SC in the Booster”, presented at the 12th Int. Particle Accelerator Conf. (IPAC’21), Campinas, Brazil, May 2021, paper WEXB08.
- [24] E. Hubbard *et al.*, “Booster Synchrotron”, FERMILAB, Batavia, IL, USA, Rep. FERMILAB-TM-405, 1973.
- [25] V. Shiltsev, “Fermilab proton accelerator complex status and improvement plans”, *Modern Phys. Lett. A*, vol. 32, p. 1730012, 2017. doi:10.1142/S0217732317300129
- [26] M. Convery *et al.*, “Fermilab accelerator complex: status and improvement plans”, FERMILAB, Batavia, IL, USA, Rep. FERMILAB-TM-2693, 2018.
- [27] M. Minty, F. Zimmermann, *Measurement and Control of Charged Particle Beams*, Berlin, Germany: Springer Nature, 2003.
- [28] E. Bravin, “Transverse beam profiles”, CERN, Geneva, Switzerland, May 2020. arXiv:2005.07400
- [29] V. Lebedev and V. Shiltsev, *Accelerator Physics at the Tevatron Collider* Berlin, Germany: Springer, 2012.
- [30] F. Roncarolo, “Accuracy of the Transverse Emittance Measurements of the CERN Large Hadron Collider”, Ph.D. thesis, Milan Polytechnic, Milan, Italy, 2005.
- [31] V. Lebedev *et al.*, “The PIP-II conceptual design report”, FERMILAB, Batavia, IL, USA, Rep. FERMILAB-TM-2649-AD-APC, 2017.
- [32] C.Y.Tan, “Ecloud in Booster”, Fermilab internal report beams-doc-9120 (Aug. 12, 2021), <https://beamdocs.fnal.gov/cgi-bin/sso/ShowDocument?docid=9120>
- [33] A. Jansson *et al.*, “Ionization Profile Monitoring at the Tevatron,” in *Proc. 10th European Particle Accelerator Conf. (EPAC’06)*, Edinburgh, UK, Jun. 2006, paper THYFI01, pp.2777-2780.
- [34] J. Zagel *et al.*, “Operational Use of Ionization Profile Monitors at Fermilab”, in *Proc. 14th Beam Instrumentation Workshop (BIW’10)*, Santa Fe, NM, USA, May 2010, paper TUPSM009, pp.111-115
- [35] J. Zagel *et al.*, “Third generation residual gas ionization profile monitors at Fermilab”, arXiv:1502.02703.
- [36] S. Antipov *et al.*, “IOTA (Integrable Optics Test Accelerator): facility and experimental beam physics program”, *Journal of Instrumentation*, vol. 12, T03002, 2017. doi:10.1088/1748-0221/12/03/T03002
- [37] J. Egberts *et al.*, “Detailed Experimental Characterization of an Ionization Profile Monitor”, in *Proc. 10th European Workshop on Beam Diagnostics and Instrumentation for Particle Accelerators (DIPAC’11)*, Hamburg, Germany, May 2011, paper WEOA03, pp. 547–549.